Representative Air Temperature of Thermally Heterogeneous Urban Areas Using the Measured Pressure Gradient

HIROFUMI SUGAWARA

Department of Geoscience, National Defense Academy of Japan, Kanagawa, Japan

KEN-ICHI NARITA

Department of Architecture Faculty of Engineering, Nippon Institute of Technology, Saitama, Japan

TAKEHIKO MIKAMI

Department of Geography, Tokyo Metropolitan University, Tokyo, Japan

(Manuscript received 13 December 2002, in final form 22 March 2004)

ABSTRACT

A method to measure an area-averaged ground air temperature based on the hydrostatic equation is shown. The method was devised to overcome the problem of finding the most representative surface air temperature over a wide region, a problem that has seriously hindered the description of urban heat islands. The vertical pressure gradient is used and the hydrostatic equation is applied to estimate the average air temperature between two barometers, which is here called the hydrostatic temperature. The error analysis shows that the hydrostatic temperature can be estimated with a systematic error of 1.8°C and a random error of 0.7°C in the case in which the two barometers have a vertical separation of 228 m. The measured hydrostatic temperature agreed with the average of the directly measured temperature within 0.7°C rms. For this barometer separation, the representative area of the hydrostatic temperature was experimentally found to be a 12-km-radius circle. The size of this area decreased when the vertical separation of the barometers decreased. The hydrostatic temperature is compared with the average directly measured temperature for various areas. The maximum correlation between them occurred for a circular area with a 12-km radius centered on the pressure measurements. The size of the representative area for this method is larger than that for the direct measurement of air temperature.

1. Introduction

The urban heat island phenomenon has been studied for many years because it generally leads to urban temperatures that significantly exceed those in rural areas. Many studies now focus on the urban heat balance and its fundamental processes (Voogt and Grimmond 2000; Grimmond and Oke 1999; Sugawara et al. 2001). Results from such studies are integrated into numerical models (Kusaka et al. 2001; Masson 2000) to gain a complete physical understanding of heat islands.

The heat island intensity, which is the air temperature difference between urban and rural areas, has been investigated for many cities. Many researchers have studied specific urban heat islands to clarify their particular features (e.g., Kim and Baik 2002; Katsoulis and Theoharatos 1985). Oke (1987) showed that the heat island intensity ranges from 2° to 12°C for many cities in America and Europe, the larger values generally holding for the larger populations. However, air temperature is also greatly affected by temperature disturbances on a scale that is smaller than the city-to-rural scale. For example, Narita (1997) measured urban air temperature variations of up to 2°C for differently oriented street canyons in the summer daytime. A street canyon receives solar radiation in an amount that depends greatly on its orientation, which results in air temperature variations within the urban area that can be as large as the heat island intensity. The heterogeneous air temperature distribution in a single urban canyon was found to vary by about 1°C (Nakamura and Oke 1988; Yoshida et al. 1990). On a slightly larger scale, Clarke and Peterson (1973) found that different land use regions in an urban area have different temperatures, the difference being 1°C. In such thermally heterogeneous environments, it is difficult to determine experimentally a single air temperature that represents the whole city. Especially in urban areas, climate characteristics such as air temperature and humidity are dominated by the immediate surroundings (Oke 1999a), so that the heat island intensity

Corresponding author address: Dr. Hirofumi Sugawara, Dept. of Geoscience, National Defense Academy of Japan, 1-10-20 Hashirimizu, Yokosuka, Kanagawa 239-8686, Japan.
E-mail: hiros@nda.ac.jp

varies greatly depending on exactly where the observation point is located. This obstacle is one of the most significant for seeking the ''universal result in the urban atmosphere'' (Oke 1999b), which might be used to describe urban climate in cities throughout the world. In such thermally heterogeneous environments, the heat flux has the same problem of spatial representativity of measurement. For example, Schmid et al. (1991) showed, from their measurements in a suburban area of Vancouver, British Columbia, Canada, that the heat flux variability between two locations was as high as 25%–40%. Details of this issue in boundary layer meteorology are summarized well in Brutsaert (1998) and Mahrt (1996). The problem of spatial representativity also exists in rural areas, but it should be less serious than that in urban areas.

To address this variability in urban climate, previous studies have tried four approaches. 1) They assume that the representative temperature is the average over many points. 2) They standardize the thermal environment around the thermometer between measurement stations, both urban and rural. 3) They measure the air temperature above the urban canopy. 4) They analyze both the measured temperature and the source area or footprint (Horst and Weil 1994; Schmid 1994). However, these methods are not always sufficient for its warranty of representativity or for validity of its assumptions. The first method is appropriate and is the most common; however, it needs a large density of measurement points to achieve statistical significance, and thus it tends to be too expensive in practice. In addition, to determine the optimum density of measurement points, one must know the air temperature distribution. Because one does not know in advance how many measurement points are enough for determining the representative air temperature, the averaged temperature should usually be checked for its representativeness after the measurement. Munn (1973) described a method for checking representativeness using the correlation coefficient and its isopleths. The second method (standardizing) is usually used at fixed meteorological stations. For example, the standard for the Japan Meteorological Agency (JMA) is that the thermometers should be 1.5 m above a lawn with an area of at least 600 m^2. With this standard, the measured air temperature difference between stations would not be affected by the difference of thermal environment within about 10 m of the thermometer, and thus any temperature differences should be due to larger-scale temperature differences. This method is useful for synoptic-scale phenomena; however, it does not necessarily represent the climate of an entire city. In addition, the measured air temperature at such a station is that above an intentionally modified surface. The fundamental question here is does the air temperature above a lawn represent that of an urban area with mixed land use? The third method (a tower) would give us the air temperature averaged vertically and horizontally because of the turbulence over an urban canopy. The temperature measured at a tower would represent a wider area than that measured inside a canopy; however, it is not the air temperature inside an urban canopy layer. Therefore, when we evaluate the heat island intensity, it does not make sense to compare the tower air temperature with the rural ground air temperature because the heat island intensity in such a definition would include the difference between inside and outside of the canopy. The use of the source area or the footprint (fourth method) is one of the more promising ways to know how well measurements represent the region, that is, the representativeness of the data. Checking the source area is not enough when there is a strong heat source, for example, a large anthropogenic heat release, however. We should analyze the source area with the measured heat source strength. In addition, the source area inside the urban canopy also increases the cost of the calculation because we have to calculate an airflow inside the urban canopy layer.

We propose here a method for measuring the area-averaged air temperature, and we describe how the method was tested. In a state of hydrostatic equilibrium, the temperature of the air mass can be determined from pressure measurements at two altitudes. This pressure-derived temperature is more representative of the air temperature than the directly measured point temperature, because air pressure is more horizontally uniform than the air temperature. Pressure perturbations directly cause airflows that tend to reduce pressure nonuniformities, and thus air pressure becomes uniform more quickly than does air temperature. This pressure-driven temperature is averaged vertically between two barometers, as well as horizontally. Therefore, we will be able to measure the averaged air temperature of the urban canopy layer. Throughout the rest of this paper, we refer to this pressure-derived temperature as the hydrostatic temperature. In the first half of this paper, the estimation method, along with its measurement error and representative area, is explained. In the last half of this paper, the hydrostatic temperature is shown to be nearly equal to the area-averaged air temperature.

2. Definition and measurement of the hydrostatic temperature

a. Method

We use the hydrostatic equation and equation of state for ideal gas to obtain the area-averaged virtual temperature T_v,

$$dP = -\rho g dz \quad \text{and} \tag{1}$$

$$P = \rho R_d T_v. \tag{2}$$

Here, dP $(=p_2 - p_1)$ is the difference in pressure between two barometers separated by a vertical distance of dz $(=z_2 - z_1 > 0)$, ρ is density, g is the acceleration of gravity, and R_d is the gas constant for dry air. We

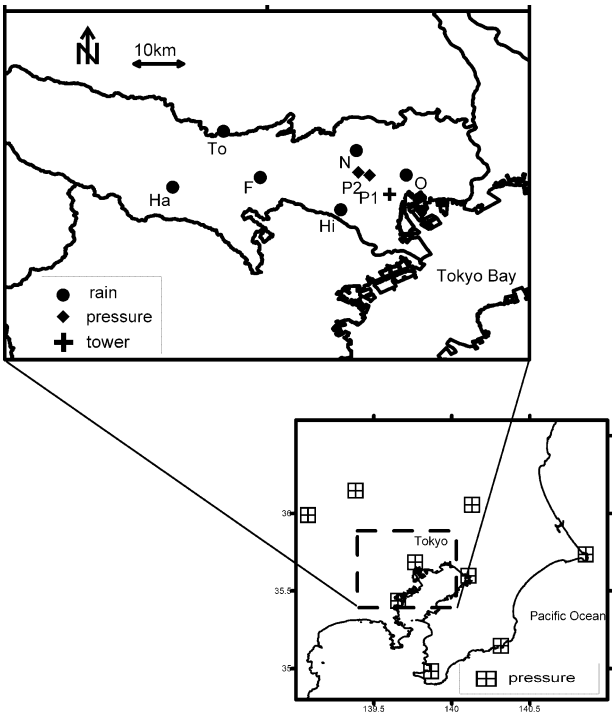

FIG. 1. Location of measurement points: P_1 is the higher-elevation site for our pressure measurements and P_2 is the lower-elevation site. The cross is the radio tower where the air temperature was measured. Closed circles are rainfall measurement sites. The crosshatched rectangles in the lower figure are sites in the pressure measurement network.

defined the reference pressure P_{ref} for the layer between P_1 and P_2,

$$P_{\text{ref}} = \frac{\int_{z_1}^{z_2} p\, dz}{\int_{z_1}^{z_2} dz}. \tag{3}$$

In this study, we equate P_{ref} to the mean air pressure of the air mass. From (2) and (3), we get the mean ρ for the layer. We get mean virtual temperature T_v from this mean ρ and (1),

$$T_v = \frac{P_{\text{ref}} g(z_2 - z_1)}{R_d(p_1 - p_2)}. \tag{4}$$

The T_v is the virtual temperature at the pressure height of P_{ref}. This T_v is not same as the mean virtual temperature from the hypsometric equation in Wallace and Hobbs (1977), even though both are derived from (1) and (2). The difference between them is discussed in section 6. By using the hydrostatic equation, we write the hydrostatic temperature T_{hyd}, the average temperature of the air mass, in terms of the area-averaged virtual temperature T_v and the specific humidity of the target air mass q as follows:

TABLE 1. Observation specifications. The absolute accuracy of the barometer is quoted from the manufacturers. The elevations are MSL, and the barometers are from Vaisala.

Site	Location	Building height (m)	Roof elev (m MSL)	Barometer	Absolute accuracy (hPa)
Upper	Shinjuku	242.5	277	PTB200A	0.20
Lower	Nakano	12.5	49	PTB220A	0.40

$$T_{\text{hyd}} = T_v/(1 + 0.608q). \tag{5}$$

Here, q is determined as an average over two altitudes. This simplification is valid because T_{hyd} is 1 order less sensitive to q than it is to the other factors, as shown later in (7). In calculating P_{ref} by (3), an exponential profile of air pressure was assumed.

b. Measurements

To evaluate this method, we compared the predicted hydrostatic temperature from the pressure gradient with direct temperature measurements in Tokyo. We focused on determining the hydrostatic temperature's accuracy and the size of its representative area.

Air pressure was measured on two building roofs in a highly built-up area of Tokyo (Fig. 1) during the summer of 1999. The building heights were 277 m above mean sea level (MSL) for the upper site (P1 in Fig. 1) and 49 m MSL for the lower site (P2 in Fig. 1). The horizontal distance between them was 1.9 km. The observation specifications are listed in Table 1, and a schematic of the region is in Fig. 2. At both sites, air temperature, relative humidity, and wind speed were also measured.

As an application of the hydrostatic temperature, we may use it as a representative air temperature of the urban canopy layer. The barometers should be set at the

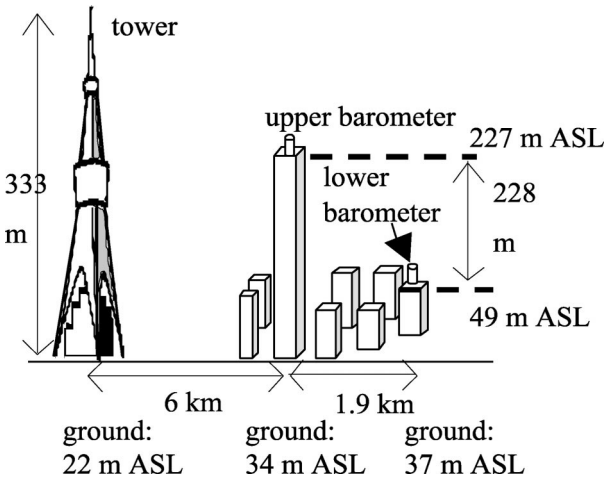

FIG. 2. Relative positions of the barometers. Both barometers are 0.05 m above the roof surface. (ASL indicates above mean sea level.)

rooftop and the canopy bottom (i.e., street level) to evaluate the representative temperature in the canopy layer. In this study, however, our goal is to evaluate the feasibility of the hydrostatic temperature. We decided to focus on the average air temperature of the air mass above the urban canopy for the following two reasons. 1) We avoid the problem of determining the dynamic pressure at the canopy bottom where the wind passing around buildings can complicate the pressure measurements. 2) We could not obtain the true averaged temperature in a canopy layer as a reference to compare with the evaluated hydrostatic temperature. The air temperature measured at the tower, on the other hand, should represent a wider area than that inside the canopy. Thus, we compare the evaluated hydrostatic temperature with the air temperature measured at the tower.

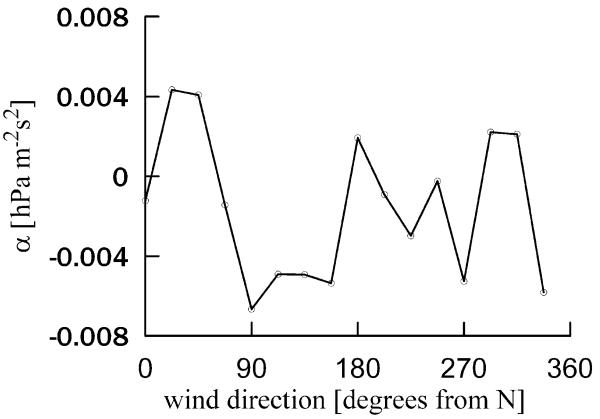

FIG. 3. Coefficient of the dynamic pressure correction for each wind direction.

c. Correction for the dynamic pressure

The static pressure gradient is needed to calculate the hydrostatic temperature, but there is generally some wind during the pressure measurement. Thus, the measured pressure is actually the static plus the dynamic pressure, the latter of which is influenced by the airflow around the barometer. The dynamic pressure for our rooftop barometers was influenced by 1) the shape of the inlet of the barometer and 2) the airflow around the building, which should decrease the measured pressure. To solve the first problem, a nondirectional, single-board-type inlet was used with the barometer (Nishiyama and Bedard 1991). Two barometers were calibrated outdoors with this inlet based on 8784 measurements, and the resulting calibration error was 0.016 hPa (standard deviation). For the second contribution to the dynamic pressure, this contribution to the dynamic pressure can be written

$$\delta P = \alpha u'^2. \quad (6)$$

Here, δP is the dynamic pressure due to the airflow $u' = u - u_{\text{av}}$, where u is the wind speed and u_{av} is the average wind speed, and α is a constant that depends on the roof structure and location of the anemometer. To determine α, we calculated u' and δP as the deviations from 30-min averages of the measured wind speed and pressure. This calculation was done for each wind direction. The coefficient α at the upper site (Fig. 3) can be positive or negative because the upper-site building had a complex roof structure. The error in α to fit the observed dP and u' in (6) is 1.44×10^{-7} hPa. For this estimate, the error was averaged over all wind directions, with the weight for each wind direction given by the occurrence frequency over the observation campaign. The errors at the upper and lower sites are included in the error evaluation shown later.

d. Correction for horizontal pressure gradients

The best sites available were separated by 1.9 km, which is not ideal for measuring the vertical pressure gradient because horizontal pressure gradients will be mistaken for vertical gradients and, thus, will cause error in the predicted hydrostatic temperature. However, according to our analyses based on the altitude-corrected data from the JMA measurement network (Fig. 1), the horizontal gradient between sites P1 and P2 in Fig. 1 was usually about 1.7×10^{-5} hPa, which is smaller than the other factors that are described later. Therefore, the horizontal gradient was neglected in this study.

e. Averaging period

The interval of each pressure measurement was 1 min at the lower site and 10 s at the upper site, which were much longer than the barometer response time. To ensure accuracy in (4), the pressure data must be time averaged because the hydrostatic equation assumes no vertical flow. Thus, the equation is more accurate when averaged over a time in which the average vertical flow is negligible. On the other hand, if the averaging period is too long, the thermal structure of the atmosphere can change during the measurement, which would complicate the analysis. However, our analysis of the power spectrum of the pressure at 10-s intervals indicated a wide range of measurement durations that would give suitable averages without averaging out meaningful pressure trends. Thus, we decided to use 10-min averages. Based on the discussion above, the estimated hydrostatic temperature represents a 10-min average. This is short enough to study the diurnal variation of air temperature and also to study thermally heterogeneous phenomena in an urban climate, for example, the temperature changes observed when a sea breeze blows into an urban area.

3. Error analysis

Based on our measurement and correction described in the previous sections, the accuracy of the hydrostatic temperature T_{hyd} was evaluated as

$$\left|\frac{\delta T_{\mathrm{hyd}}}{T_{\mathrm{hyd}}}\right| = \left|\frac{\delta T_v}{T_v}\right| + \frac{0.608}{1 + 0.608q}|\delta q|$$

$$\approx \left|\frac{\delta T_v}{T_v}\right| + 6.1 \times 10^{-1}|\delta q| \quad \text{and} \qquad (7)$$

$$\left|\frac{\delta T_v}{T_v}\right| = \left|\frac{\delta P_{\mathrm{ref}}}{P_{\mathrm{ref}}}\right| + \left|\frac{\delta dz}{dz}\right| + \left|\frac{\delta dP}{dP}\right|. \qquad (8)$$

Here, δX is the error of value X when X is T, P, z, or q. Each systematic error is due to the absolute accuracy of measurements and would result in a bias error of the hydrostatic temperature. The random errors were obtained as a standard deviation of the measured means. The random errors produce fluctuations of the hydrostatic temperature:

$$\frac{\delta P_{\mathrm{ref}}}{P_{\mathrm{ref}}} = \frac{3.5}{1000} = 3.5 \times 10^{-3}\,(\text{systematic error}) \quad \text{and} \qquad (9)$$

$$\frac{\delta P_{\mathrm{ref}}}{P_{\mathrm{ref}}} = \frac{1.1}{1000} = 1.1 \times 10^{-3}\,(\text{random error}), \qquad (10)$$

where δP_{ref} was estimated from (3) and the instrument errors from the manufacturers;

$$\frac{\delta dP}{dP} = \frac{6.1 \times 10^{-3}}{25} = 2.4 \times 10^{-4}\ \text{(systematic)} \quad \text{and} \qquad (11)$$

$$\frac{\delta dP}{dP} = \frac{3.2 \times 10^{-2}}{25} = 1.2 \times 10^{-3}\ \text{(random)}, \qquad (12)$$

where δdP was estimated from the results of cross calibration of two barometers and the dynamic pressure correction (previously shown in the section 2c);

$$\frac{\delta dz}{dz} = \frac{0.5}{228} = 2.2 \times 10^{-3}\ \text{(systematic)} \quad \text{and} \qquad (13)$$

$$\frac{\delta dz}{dz} = 0\ \text{(random)}, \qquad (14)$$

where dz and δdz were determined from the building construction drawings; and

$$\delta q = 1.3 \times 10^{-4}\ \text{kg kg}^{-1}\ \text{(systematic)} \quad \text{and} \qquad (15)$$

$$\delta q = 2.5 \times 10^{-5}\ \text{kg kg}^{-1}\ \text{(random)}, \qquad (16)$$

where δq was estimated from the instrument error. The heterogeneity of humidity is not considered here; it depends on the circumstance of the observation area. In the circumstance of heavy heterogeneity in humidity, like advection from sea, the error should be increased. However, T_{hyd} is 1 order less sensitive than the other error factors as shown in (7). For example, in summer time in Tokyo, Japan, sea-breeze advection could cause 1 g kg^{-1} of variation in specific humidity, which corresponds to 10% of the absolute value. If δq increases 1 g kg^{-1}, the δT_{hyd} increases from 1.8° to 2.0°C. As a result, the total errors are

$$\left|\frac{\delta T_{\mathrm{hyd}}}{T_{\mathrm{hyd}}}\right| = 5.9 \times 10^{-3}\ \text{(systematic)} \quad \text{and} \qquad (17)$$

$$\left|\frac{\delta T_{\mathrm{hyd}}}{T_{\mathrm{hyd}}}\right| = 2.3 \times 10^{-3}\ \text{(random)}. \qquad (18)$$

When $T_{\mathrm{hyd}} = 300$ K,

$$\delta T_{\mathrm{hyd}} = 1.8\ \text{(systematic)} \quad \text{and} \qquad (19)$$

$$\delta T_{\mathrm{hyd}} = 0.7\ \text{(random)}. \qquad (20)$$

Thus, the resulting hydrostatic temperature can have a 1.8°C bias error and a 0.7°C random error, which is less accurate than measurements from typical thermometers. However, improvements in barometer accuracy and dynamic pressure correction should increase the accuracy.

4. Size of the averaged area

How large an area does this hydrostatic temperature represent? In physical terms, we expect that the representative area should increase with an increase in the vertical separation of the barometers. However, this effect is hard to predict quantitatively, and so we determined experimentally the detection range of the barometer instead of the average area. In rainy conditions, the density of air mass increases because of the weight of the raindrops. The measured pressure gradient is the sum of the weight of air and raindrops. Therefore, in rainy conditions, the hydrostatic temperature obtained from this increased pressure gradient is lower than the directly measured air temperature. It is possible to determine the detection range by analyzing the distribution of the rainy areas around the observation sites. The difference due to the raindrops was larger than that from the thermal heterogeneity, which also contributes to the temperature differences. This detection range should not change according to the weather condition. Thus, we treat this detection range as an average area of the hydrostatic temperature on clear days.

Rainy areas were detected by radar and rain gauge data in this study. We assumed that areas with radar echo intensities of 20 dB or larger were raining areas. There are two uncertainties with use of the radar. First, the radar echo does not always coincide with rainy areas. Second, to avoid ground clutter of radio waves, the radar echoes used here were 2-km-high constant-altitude plan position indicators (CAPPI), which were above the target air mass of the barometers. Disagreement between the radar echo and the actual rainy areas was supplemented by simultaneous analysis of rain gauge data. Figure 4 shows one example of radar echo distribution on 24 August 1999. Figure 5 shows the evaluated hydrostatic temperature T_{hyd}, the directly measured temperature at the station O (in Fig. 1) T_O, and the precipitation amount. The temperatures are shown in the form of potential temperature. Three sets of precipitation data are shown, and each is the average of two data points.

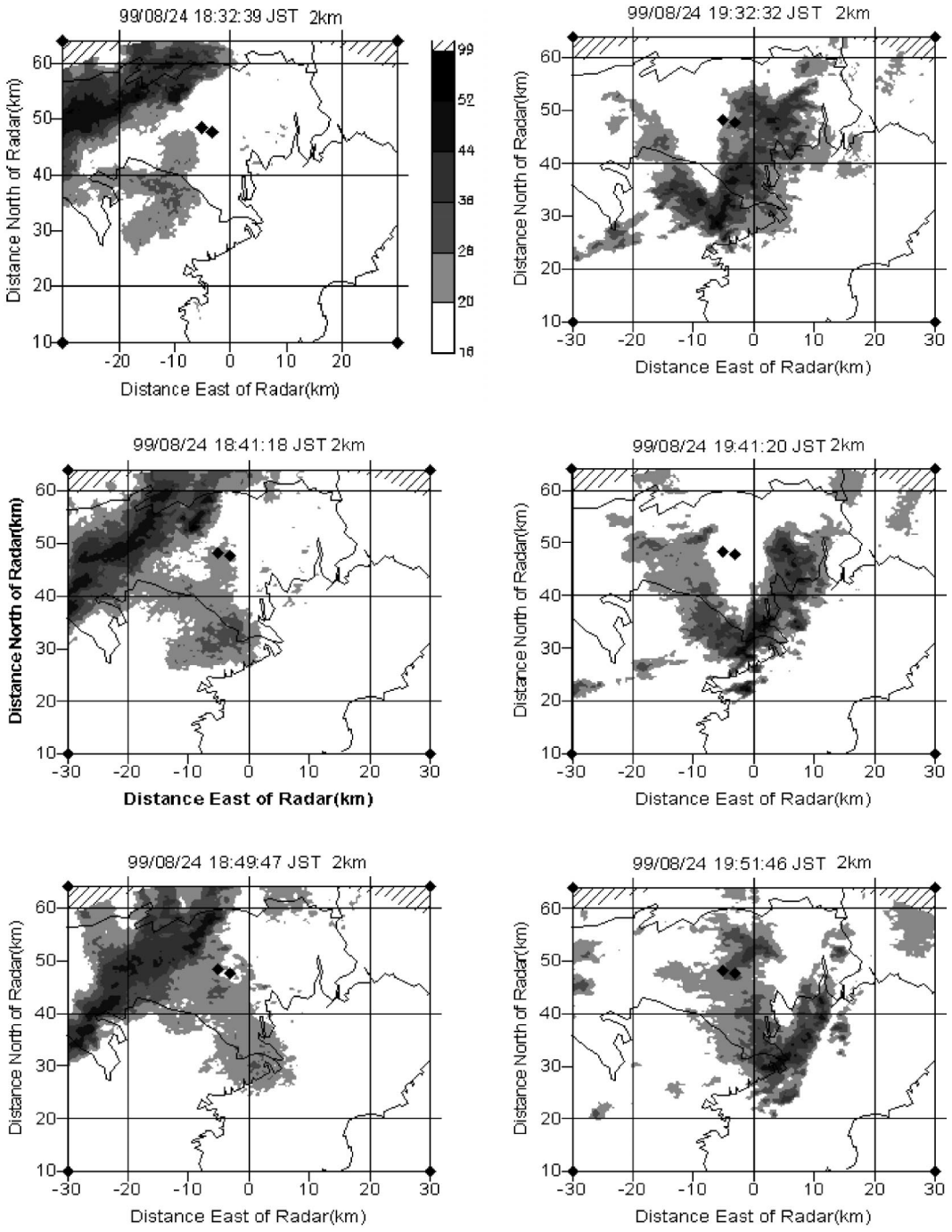

FIG. 4. Radar echo distribution around the observation sites on 24 Aug 1999 from the CAPPI image at 2 km MSL. The grayscale shows the radar echo intensity (dBZ). The two diamonds mark the pressure measurement sites.

These groups of rain gauge stations were determined according to the shape of the radar echo. As is shown in both the radar echo and the precipitation, the raining area moved from northwest toward the southeast, passing through the pressure measurement sites. The precipitation time series were consistent with the radar echo distribution. The radar echo distribution at 1941 Japan standard time (JST) in Fig. 4 shows no echo around the barometers. This echo-free situation is consistent with the smaller temperature difference between the hydrostatic and directly measured temperatures in Fig. 5. This result suggests that the barometers could not detect the rain area around them at 1941 JST. Therefore, the area represented by the pressure measurements should be

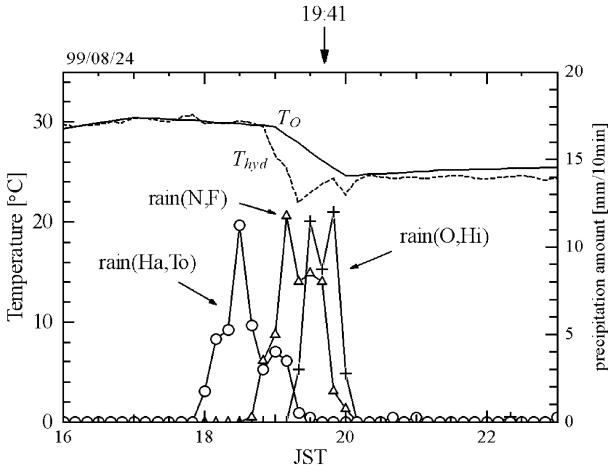

FIG. 5. Temperature time series during the rainy period on 24 Aug 1999. The hydrostatic temperature T_{hyd} and the directly measured temperature T_O are plotted as potential temperatures. Precipitation amount is shown on the right axis. Each precipitation curve is the average of the two measurement points labeled in parentheses. Refer to Fig. 1 for the locations of these measurement points.

equal to or less than the echo-free area. A total of eight cases were analyzed, and the resulting representative area had a radius of 12.3 km around the barometers. The number of cases is limited to only eight cases because we used the distance between the barometers and the echo edge. To determine the detection range with this method, we need an echo of adequate shape that is isolated from the other echoes. The standard deviation was 1.7 km. In this case, the representative area was much larger than that of the direct measurement of temperature (about 100 m or less) and was larger than the scale of thermal heterogeneity.

To see how this representative area depends on the vertical distance between two barometers, we used two other sets of observations. These sets also used tall buildings and continued for about 1 month. The barometer height differences *dz* were 24 and 123 m. Table 2 shows that the averaged area is larger for greater height differences. The range of detection could not be determined for a height difference of 24 m, because this measurement resulted in an unrealistic value for the hydrostatic temperature. Therefore, a vertical distance longer than 24 m is needed, at least for the barometers we used (i.e., pressure gradient accuracy of 0.016 hPa).

5. Evaluation of the hydrostatic temperature

In this section, we compare T_{hyd} with the directly measured air temperatures. This comparison is consistent with our estimated accuracy and also indicates that the hydrostatic temperature represents the temperature of the air mass above the urban canopy.

These comparison temperatures were measured on a 333-m-high radio tower 6 km away from the pressure measurement sites (Fig. 1). This 6-km distance is close enough because the radius of the averaged area is 12.3 km. These air temperatures are routinely measured for the Tokyo Metropolitan Bureau. Because the measured hydrostatic temperature here is designed to represent the air mass above the urban canopy (Fig. 2), we compared the hydrostatic temperature with the tower air temperature at 86 and 191 m MSL (Fig. 6). These heights are 64 and 169 m above ground level (AGL), respectively, and the mean height of the buildings around the tower is 10 m. The tower temperature at both heights can represent the region above the urban canopy because 1) they are above the roughness sublayer of the urban canopy and 2) the source area of the measured temperature at 169 m AGL extends an average of 1000 m along the wind direction, according to the estimation method in Schmid (1994). The tower data were measured during 29 July–4 August 1999, which were all clear days. To avoid a change of temperature caused by a change of reference height, we transformed all of the temperatures into the potential temperature. The two measures of temperature agree within the estimated error of the hydrostatic temperature. Table 3 lists the averaged difference (bias) and the rms difference. These values were calculated from the data in Fig. 6. The rms differences are less than or nearly equal to 0.7°C, the calculated random error of the hydrostatic temperature, whereas the biases

TABLE 2. Range of detection for the hydrostatic temperature. The range of detection could not be determined for a height difference of 24 m.

dz (m)	24	123	228
Range of detection (std dev) (km)	—	7.3 (0.7)	12.3 (1.7)

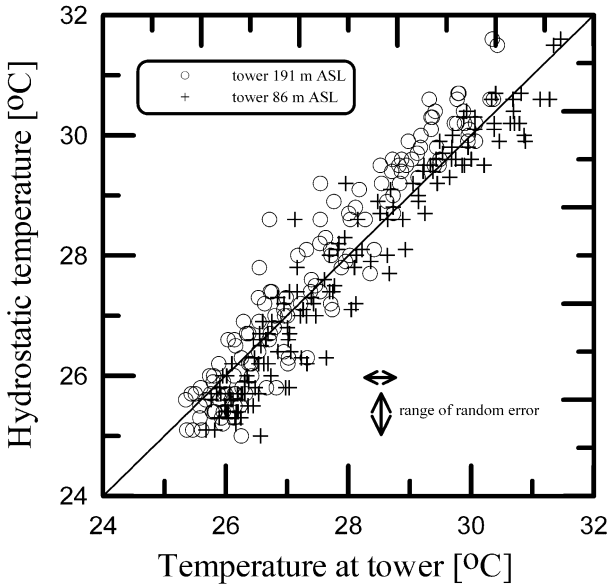

FIG. 6. Comparison between the hydrostatic temperature and the directly measured temperature at two heights on the tower. All temperatures are potential temperatures.

TABLE 3. Difference (°C) between the hydrostatic temperature and the directly measured temperature on the tower. The averaged difference (bias) and rms differences are shown. The statistics are calculated on the potential temperature differences for fair-weather days (29 Jul–4 Aug 1999). The heights are MSL, and the bias shows the tower minus hydrostatic temperature.

Height (m)	86	125	191	227	272
Bias					
Day	0.08	−0.48	−0.63	−0.50	−0.55
Night	0.66	0.42	0.38	0.56	0.37
Rms					
Day	0.47	0.66	0.76	0.67	0.70
Night	0.89	0.73	0.70	0.82	0.69

are much less than the calculated value of 1.8°C. Therefore, we conclude that our measurement of the hydrostatic temperature is justified.

On the other hand, near tower temperatures of 26°C, the hydrostatic temperature is generally lower than the temperature at 86 m AGL (Fig. 6). In Table 3, both the bias and rms at 64 m AGL at night are larger than those of the daytime. This day-to-night difference is significant in comparison with those of other heights. To clarify this difference, we analyzed the diurnal variation. Figure 7 shows the diurnal variation of the hydrostatic temperatures, the tower air temperature at 86 m, and the rooftop air temperature. The rooftop temperature is the average of three sites around the tower. The hydrostatic temperature is lower than that at 86 m at night, but it is nearly equal to the rooftop air temperature. We found that the hydrostatic temperature at night was lower than the air temperature inside the urban canopy (not shown here). The cool layer at roof level is likely due to the radiation cooling on the roof surface. The temperature inside the canopy remains high because there is less radiational cooling at night. Although the roof-level temperature is the average of only three sites, the data indicate that the hydrostatic temperature is more influenced by roof-level temperature than by those at other heights. The cold layer with high density has more influence on the hydrostatic temperature than does the warmer (lower density) layer, because the hydrostatic temperature was acquired from the density of the air mass (i.e., through the pressure gradient). Therefore, the hydrostatic temperature might be greatly affected by this cool, high-density layer at the roof level.

Now we address the horizontal representativeness of the hydrostatic temperature. We compared the hydrostatic temperature and the directly measured air temperature at surface observation sites. The directly measured temperatures are averaged according to their distance from the pressure measurement site,

$$T_{\mathrm{av}}(r) = \frac{1}{n}\sum_{i} T_i(d) \quad \text{for } d < r. \tag{21}$$

Here, $T_i(d)$ is the directly measured temperature at distance d from the pressure measurement site (P1 in Fig. 1). Temperature $T_{\mathrm{av}}(r)$ is evaluated for $r = 4, 6, 8, 10, \ldots, 32$, and 34 km. The interval of r is determined with consideration of the measurement site density. The

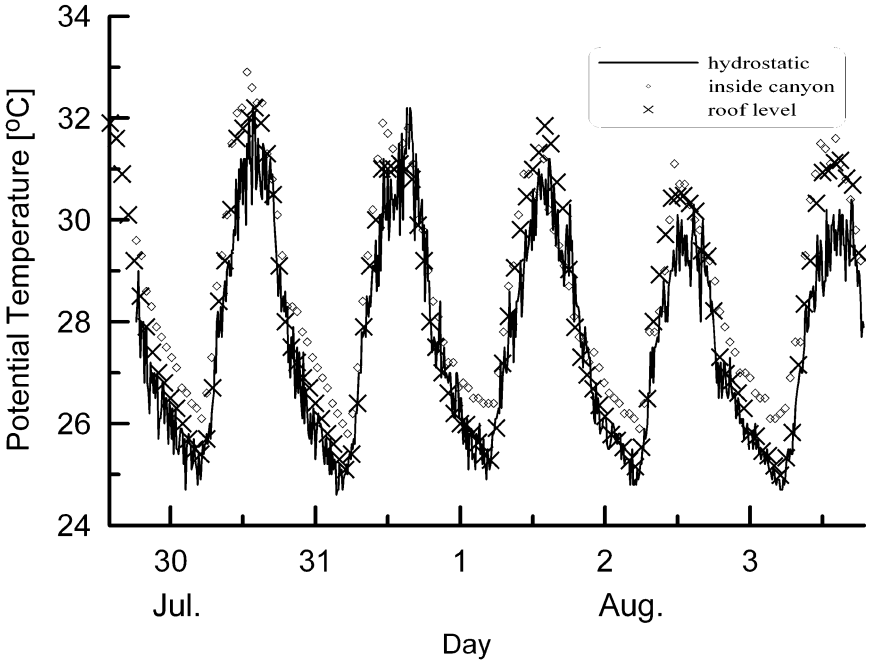

FIG. 7. Temperature times series during fair-weather days (29 Jul–4 Aug 1999). All temperatures are potential temperatures. The hydrostatic temperature and the direct measurements at 86 m and the rooftop (average of three sites) are shown.

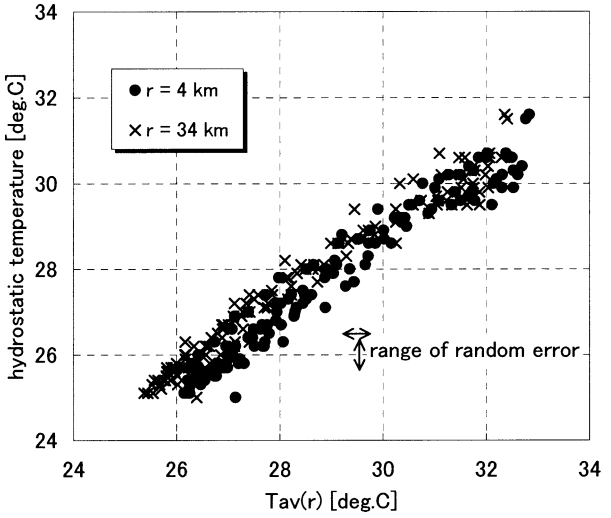

FIG. 8. Comparison of the hydrostatic temperature with the average temperature $T_{av}(r)$ from surface observation sites. The latter is averaged over the sites within $r = 4$ and 34 km of the pressure observation site.

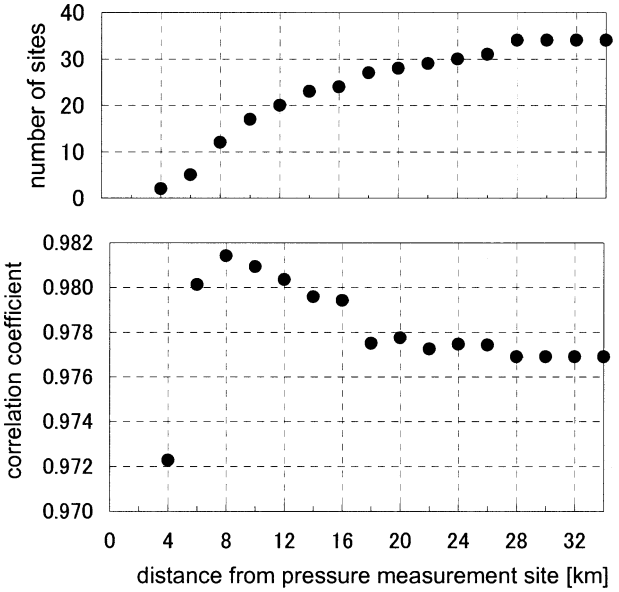

FIG. 9. (top) Number of temperature measurement sites within radius r of the pressure measurement site, and (bottom) the correlation coefficient between the hydrostatic temperature and the average temperature $T_{av}(r)$ of these sites. The horizontal axis is the distance r from the pressure measurement sites inside of which the temperatures were used to calculate $T_{av}(r)$.

data from a total of 34 surface sites were used. These sites are routine observatories of the JMA and the Tokyo Metropolitan Bureau. Some of them are located on roofs, and others are at street level. Because the hydrostatic temperature was determined for the air mass above the urban canopy layer, we do not expect absolute agreement between the hydrostatic temperature and $T_{av}(r)$. However, we argue that the correlation between T_{hyd} and T_{av} is highest when the temperatures are measured within the representative area. Mikami et al. (1999) showed the air temperature distribution in Tokyo with more measurement stations (1/10.5 km^2) than that used here (1/22 km^2). Shimoyama (1996) also used more stations (1/2.5 km^2). Their isopleths showed the typical temperature distribution of a concentric circle. Considering the contour interval of their isopleths and the number of stations in calculating $T_{av}(r)$, the $T_{av}(r)$ should be representative of the area with the error of standard deviation, which is 0.6°C for $d = 12$ km.

Figure 8 shows the correlation between the hydrostatic temperature and $T_{av}(d)$ at $d = 4$ and 34 km. Here, $T_{av}(d)$ is 1.0°–2.0°C higher than the hydrostatic temperature but is approximately proportional to T_{hyd}. The coefficient of determination is $R^2 = 0.94$ for 4 km and 0.96 for 34 km, which indicates good correlation. The degree of scatter is roughly independent of temperature, and the rms difference from the linear regression was 0.48°C for 4 km and 0.47°C for 34 km, which is less than the estimated random error of 0.7°C.

Figure 9 shows that the correlation coefficient has a local maximum for 6 km $< r <$ 16 km. This indicates that the hydrostatic temperature is the representative temperature for the surface area within 6–16 km of the measurement site. In section 4, the representative area was evaluated as having a radius of 12 km. The agreement between these values is encouraging because they were obtained independently.

We conclude that the hydrostatic temperature can accurately represent the vertical and horizontal average of the air mass. It agreed with the tower-measured air temperature within the error range of the hydrostatic temperature estimation, and its bias error was less than the predicted error. This agreement was not as good at night, although the discrepancy was likely caused by a radiatively cooled layer at the rooftop. In the horizontal, the area in which the hydrostatic temperature correlated best with the measured average temperature was for sites within 6–16 km of the pressure measurements. There are only 20 sites for 12-km scale, and the average of these sites might miss the true area average for its statistical significance. Nevertheless, to the extent of this site density, the hydrostatic temperature was shown to be the mean air temperature in the horizontal within the predicted error range.

6. Discussion

a. Comparison with the hypsometric equation

The mean virtual temperature can be calculated also from the hypsometric equation (Wallace and Hobbs 1977):

$$z_2 - z_1 = \frac{R_d T_v}{g} \ln\left(\frac{p_1}{p_2}\right). \qquad (22)$$

Here, we denote this virtual temperature as T_{vpsm},

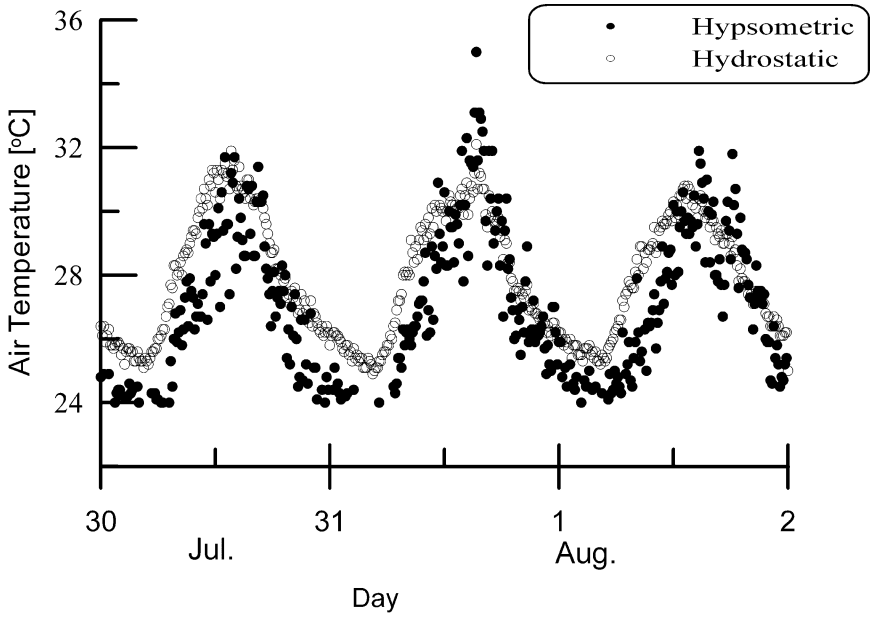

FIG. 10. Time series of hypsometric temperature during fair-weather days. The hydrostatic temperature is also shown. Both temperatures are air temperatures, not potential temperatures.

$$T_{v\text{psm}} = \frac{g(z_2 - z_1)}{R_d \ln(p_1/p_2)}. \tag{23}$$

The difference between T_v in (4) and $T_{v\text{psm}}$ is the term $P_{\text{ref}}/(p_1 - p_2)$in (4) and $1/\ln(p_1/p_2)$ in (23). The latter is the integration of the former. Therefore, the T_v is calculated from the broad-layer gradient of pressure between the barometers. On the other hand, (23) calculates $T_{v\text{psm}}$ from the integration of the local gradient. Another difference is that the T_v is more robust for the error of barometers than $T_{v\text{psm}}$. The T_v depends on the relative accuracy of two barometers, however, $T_{v\text{psm}}$ depends on the absolute accuracy of each barometer. The accuracy of the air temperature T_{psm} that is calculated from the hypsometric equation is evaluated as

$$\left|\frac{\delta T_{\text{psm}}}{T_{\text{psm}}}\right| = \left|\frac{\delta dz}{dz}\right| + \left|\frac{1}{\ln(P_1/P_2)}\left(\frac{\delta P_1}{P_1} + \frac{\delta P_2}{P_2}\right)\right| + 6.1 \times 10^{-1}|\,\delta q|. \tag{24}$$

We evaluate δP_1 and δP_2 as 0.1 hPa for the systematic error based on the manufacturer's report. The random error was obtained as a standard deviation of the measured means, 3.16×10^{-2} hPa. Thus,

$$\left|\frac{\delta T_{\text{psm}}}{T_{\text{psm}}}\right| = 1.0 \times 10^{-2} \text{ (systematic)} \quad \text{and} \tag{25}$$

$$\left|\frac{\delta T_{\text{psm}}}{T_{\text{psm}}}\right| = 2.54 \times 10^{-3} \text{ (random)}. \tag{26}$$

When $T_{\text{psm}} = 300$ K,

$$\delta T_{\text{psm}} = 3.1 \text{ (systematic)} \quad \text{and} \tag{27}$$

$$\delta T_{\text{psm}} = 0.8 \text{ (random)}. \tag{28}$$

The systematic error is 1.7 times that of the hydrostatic temperature (T_{hyd}) shown in (19). The pressure difference for the two barometers was carefully calibrated in this study; therefore, the T_{hyd} is more accurate than T_{psm}. Figure 10 shows the diurnal variation of the T_{psm} and the T_{hyd}. Because of the larger random error, the T_{psm} fluctuation is considerable. A difference at nighttime, which is within the range of systematic error, might be caused by the cooled layer at the roof level, as shown in section 5.

b. Error factors

Among the error factors in (9)–(16), P_{ref} is the largest. For the absolute pressure measurements, the dynamic pressure correction was the greatest source of error. This dynamic pressure is caused by 3D airflow around the barometer that will vary from site to site, depending on the complex airflow around the nearby buildings. Therefore, to obtain an accurate hydrostatic temperature, one has to determine the airflow and dynamic pressure in the urban canyon around the barometer. Progress in the dynamic pressure correction would make it possible to evaluate the hydrostatic temperature of urban canopy layer. At present, a large source of systematic error is the height measurement [(13)]. The GPS survey technique or a laser range meter would reduce this error, for example, if the height was known to within 10 cm, for our case with $dz = 228$ m, then this source of error would be negligible.

c. Comparison of the hydrostatic temperature with the other normal measurements

Here we compare the hydrostatic temperature with the four methods of measuring the representative temperature measurement that we mentioned in the introduction. As compared with taking the average of many measurement points whose thermal environments are standardized, the hydrostatic temperature has the advantage of requiring fewer measurement points. Putting the thermometers on a tower is a promising method. The source area of air temperature measured at 250 m AGL on the tower was 2.5 km or less, a value that depends on the tower height and meteorological conditions. This area is smaller than that of the hydrostatic temperature (12.3 km), with a vertical separation of 228 m. Acoustic tomography is another measurement method of area-averaged temperature (Gerd et al. 2002; Funakoshi et al. 2000). This method uses the travel time of sound to determine the temperature averaged along the sound path rather than the 3D air mass of the hydrostatic temperature.

7. Conclusions

The representativeness of the measured ground air temperature is a big uncertainty in studies of urban heat islands. Air temperatures in urban areas vary widely with the measurement point, and can be as much as the temperature difference between the urban and surrounding rural areas. We have argued that area-averaged temperatures based on the hydrostatic equation and the vertical pressure gradient can accurately represent the temperature of the urban air mass. In this method, one measures the pressure at two altitudes, and the inferred hydrostatic temperature is the average air temperature of the air mass between the barometers.

We compared the hydrostatic temperature to direct measures of temperature. To make this comparison, we installed barometers on two buildings with different heights and continually measured the pressures for about 1 month for each of three datasets. The hydrostatic temperature was shown to be an average of the air mass. For the 228-m vertical separation, T_{hyd} deviated from the directly measured temperature when rain fell within 12.3 ± 1.7 km of the pressure measurements, which provides a range of the representative temperature. This distance agreed with the higher correlation between T_{hyd} and the directly measured temperatures when the latter were within 6–16 km of the pressure measurements. For the 123-m separation, this deviation of T_{hyd} from the directly measured temperature was significant only when rain was within 7.3 ± 0.7 km of the pressure measurements. Thus, the two independent measures of representative area were consistent, and this area decreased when the barometers were closer together (from 12.3 to 7.3 km). When the vertical separation was 123 or 228 m, the size of representative area was 7.3 or 12.3 km, respectively, which is much larger than that of the direct measurement (about 100 m or less in the urban canopy layer, or about 1 km or less for the tower thermometer).

The error analysis showed that the hydrostatic temperature can be estimated with a systematic error of 1.8°C and a random error of 0.7°C when the barometers were separated vertically by 228 m. The errors are smaller than those of the other pressure-derived air temperature that is calculated from the hypsometric equation. The hydrostatic temperature was measured to be closer to the area average of the directly measured temperature than the predicted error. Nevertheless, the systematic and random errors should be reduced for studies of urban climate. Because the largest error is from the pressure measurement, particularly from the dynamic pressure, more accurate estimates of the hydrostatic temperature should reduce the uncertainties caused by the dynamic pressure.

Improvement of pressure measurement techniques would make this hydrostatic temperature valuable in thermally heterogeneous urban areas where determining the representative temperature is problematic, because this method has a wide representative area.

Acknowledgments. We thank the anonymous reviewers for their useful comments and suggestions. This study was financially supported by CREST of the Japan Science and Technology Cooperation.

REFERENCES

Brutsaert, W., 1998: Land-surface water vapor and sensible heat flux: Spatial variability, homogeneity, and measurement scales. *Water Resour. Res.,* **34,** 2433–2442.

Clarke, J. F., and J. T. Peterson, 1973: An empirical model using eigenvectors to calculate the temporal and spatial variations of the St. Louis heat island. *J. Appl. Meteor.,* **12,** 195–210.

Funakoshi, A., K. Mizutani, K. Nagai, K. Harakawa, and T. Yokoyama, 2000: Temperature distribution in circular space reconstructed from sampling data at unequal intervals in small numbers using acoustic computerized tomography (A-CT). *Japan. J. Appl. Phys.,* **39,** 3107–3111.

Gerd, T., K. Arnold, A. Raabe, and A. Ziemann, 2002: Observations of area averaged near-surface wind- and temperature-fields in real terrain using acoustic travel time tomography. *Meteor. Z.,* **11,** 273–283.

Grimmond, C. S. B., and T. R. Oke, 1999: Heat storage in urban areas: Local-scale observations and evaluation of a simple model. *J. Appl. Meteor.,* **38,** 922–940.

Horst, T. W., and J. C. Weil, 1994: How far is far enough?: The fetch requirements for micrometeorological measurement of surface fluxes. *J. Atmos. Oceanic Technol.,* **11,** 1018–1025.

Katsoulis, B. D., and G. A. Theoharatos, 1985: Indications of the urban heat island in Athens, Greece. *J. Appl. Meteor.,* **24,** 1296–1302.

Kim, Y. H., and J. J. Baik, 2002: Maximum urban heat island intensity in Seoul. *J. Appl. Meteor.,* **41,** 651–659.

Kusaka, H., H. Kondo, Y. Kikegawa, and F. Kimura, 2001: A simple single-layer urban canopy model for atmospheric models: Comparison with multi-layer and slab models. *Bound.-Layer Meteor.,* **101,** 329–358.

Mahrt, L., 1996: The bulk aerodynamic formulation over heterogeneous surfaces. *Bound.-Layer Meteor.,* **78,** 87–119.

Masson, V., 2000: A physically-based scheme for the urban energy budget in atmospheric models. *Bound.-Layer Meteor.,* **94,** 357–397.

Mikami, T., A. Kannari, Y. Yamazoe, C. Suzuki, K. Kimura, and S. Kubo, 1999: Investigation of urban heat islands in Tokyo metropolis based on the ground monitoring system. *Proc. Int. Conf. on Urban Climatology,* Sydney, Australia, WMO, CD-ROM, ICUC10.3.

Munn, R. E., 1973: Urban meteorology: Some selected topics. *Bull. Amer. Meteor. Soc.,* **54,** 90–93.

Nakamura, Y., and T. R. Oke, 1988: Wind, temperature and stability conditions in an east–west oriented urban canyon. *Atmos. Environ.,* **22,** 2691–2700.

Narita, K., 1997: Annual observation on the temperature field in Hiroshima city. *Proc. Second Japanese–German Meeting,* Kobe, Japan, Kobe University, 243–246.

Nishiyama, R. T., and A. J. Bedard Jr., 1991: A ''quad-disc'' static pressure probe for measurement on adverse atmospheres: With a comparative review of static pressure prove designs. *Rev. Sci. Instrum.,* **62,** 2193–2204.

Oke, T. R., 1987: *Boundary Layer Climate.* Halsted Press, 372 pp.

——, 1999a: Observing urban weather and climate using 'standard' stations. *Proc. Int. Conf. on Urban Climatology,* Sydney, Australia, WMO, CD-ROM, ICUC3.3.

——, 1999b: On the search for 'universal results' in the urban atmosphere. *Proc. Int. Conf. on Urban Climatology,* Sydney, Australia, WMO, CD-ROM, ICUC8.1.

Schmid, H. P., 1994: Source area for scalars and scalar fluxes. *Bound.-Layer Meteor.,* **67,** 293–318.

——, H. A. Cleugh, C. S. B. Grimmond, and T. R. Oke, 1991: Spatial variability of energy fluxes in suburban terrain. *Bound.-Layer Meteor.,* **54,** 249–276.

Shimoyama, H., 1996: Daytime air temperature distribution in Tokyo on fine day (in Japanese). M.S. thesis, Dept. of Geography, Tokyo Metropolitan University, 45 pp.

Sugawara, H., K. Narita, and T. Mikami, 2001: Estimation of effective thermal property parameter on a heterogeneous urban surface. *J. Meteor. Soc. Japan,* **79,** 1169–1181.

Voogt, J. A., and C. S. B. Grimmond, 2000: Modeling surface sensible heat flux using surface radiative temperatures in a simple urban area. *J. Appl. Meteor.,* **39,** 1679–1699.

Wallace, J., and P. Hobbs, 1977: *Atmospheric Science, An Introductory Survey.* Academic Press, 57 pp.

Yoshida, A., K. Tominaga, and S. Watatani, 1990: Field measurements on energy balance of an urban canyon in the summer season. *Energy Build.,* **15,** 417–423.